Guo, R.; Neada, M.; Hakala, T. K.; Väkeväinen, A. I.; Törmä, P.

Lasing at K Points of a Honeycomb Plasmonic Lattice

Published in:
Physical Review Letters

DOI:
10.1103/PhysRevLett.122.013901

Published: 02/01/2019

Document Version
Publisher's PDF, also known as Version of record

Please cite the original version:
Guo, R., Neada, M., Hakala, T. K., Väkeväinen, A. I., & Törmä, P. (2019). Lasing at K Points of a Honeycomb Plasmonic Lattice. Physical Review Letters, 122(1), 1-6. [013901].
https://doi.org/10.1103/PhysRevLett.122.013901

Lasing at K Points of a Honeycomb Plasmonic Lattice

R. Guo,[1] M. Nečada,[1] T. K. Hakala,[1,2] A. I. Väkeväinen,[1] and P. Törmä[1,*]
[1]Department of Applied Physics, Aalto University, FI-00076 Aalto, Finland
[2]Institute of Photonics, University of Eastern Finland, P.O. Box 111, FI-80101 Joensuu, Finland

(Received 23 May 2018; published 2 January 2019)

We study lasing at the high-symmetry points of the Brillouin zone in a honeycomb plasmonic lattice. We use symmetry arguments to define singlet and doublet modes at the K points of the reciprocal space. We experimentally demonstrate lasing at the K points that is based on plasmonic lattice modes and two-dimensional feedback. By comparing polarization properties to T-matrix simulations, we identify the lasing mode as one of the singlets with an energy minimum at the K point enabling feedback. Our results offer prospects for studies of topological lasing in radiatively coupled systems.

DOI: 10.1103/PhysRevLett.122.013901

Feedback provided by a resonator is essential for lasing. The resonator can be a set of mirrors [1] or periodic structures enabling distributed feedback (DFB) lasing [2–6]. Most DFB lasers rely on simple one-dimensional periodic structures. More complex geometries would offer such interesting features as distributed feedback involving multiple modes, flat bands, and increased variety of degenerate high-symmetry points and possibilities of creating topological bands [7]. The symmetry of a hexagonal Bravais lattice leads to the possibility to multiply degenerate points at the first Brillouin zone edge [8]. Here we experimentally demonstrate lasing at K points of a honeycomb plasmonic lattice.

The vast majority of the work on bosons in hexagonal (including honeycomb) lattices for photonic [9–11], microwave [12,13], and atomic [14–17] systems realize essentially the tight-binding model of the lattice. That is, the lattice sites are connected only up to the (next-)nearest neighbor; in the optical systems, this is realized by site-to-site near-field coupling. Our system consists of an array of plasmonic nanoparticles that are radiatively coupled over the whole system size. This renders tight-binding models useless, and we base our theoretical description on symmetry arguments and T-matrix scattering simulations.

Plasmonic nanohole and nanoparticle arrays combined with organic and inorganic gain materials are emerging as a versatile platform for room-temperature, ultrafast lasing [18–32] and Bose-Einstein condensation [33,34]. These works, however, focus on lasing action or condensation at the Γ point, that is, at the center of the Brillouin zone of systems with a Bravais lattice that is rectangular or square [18–22,24–27,29], hexagonal [30,32], or one-dimensional [28] (Ref. [31] studies lasing action in the X point of a square lattice).

K-point lasing or condensation in radiatively (long-range) coupled hexagonal lattices has been studied in photonic crystal [35–37] and exciton-polariton [38] systems. In those works, however, the polarization properties of the output light were not analyzed. Here we demonstrate lasing at the K points and show that the polarization properties and real-space patterns of the laser emission contain essential information about the lasing mode. We identify the lasing mode as one of the singlets allowed by symmetry and explain why this mode is selected by the lasing action.

We fabricate cylindrical gold nanoparticles with electron-beam lithography on a glass substrate in a honeycomb lattice arrangement. The particle separation is varied between 569–583 nm. Individual nanoparticles have a nominal diameter of 100 nm and height of 50 nm. An organic dye molecule IR-792 is added on top of the array in 25 mM solution and the structure is sealed with a glass superstrate [Fig. 1(b)]. The dye molecules act as the gain material and are optically pumped with 100 fs laser pulses (750 nm central wavelength). For details, see Supplemental Material [39], which includes Refs. [40–48].

The energies of diffracted orders (DOs) of a 2D hexagonal lattice are shown with dashed lines in Fig. 1(a) for the Γ–K in-plane (x–y plane) momentum direction. The DOs correspond to diffraction without resonant phenomena at the lattice sites, so-called empty lattice approximation. In our samples, the nanoparticles have a broad plasmonic resonance (at 1.87 eV, width ~300 meV), which hybridizes with the DOs, leading to narrow (width 5–20 meV) dispersive modes called surface lattice resonances (SLRs) [49,50], see Fig. 1(a). A dispersion obtained by multiple-scattering T-matrix simulation (for details, see Ref. [24] and the Supplemental Material [39]) agrees with the experiments, see the insets of Fig. 1(a). The dispersions are measured with a Fourier imaging setup used in our previous works [24,34,51] but are now extended to larger angles.

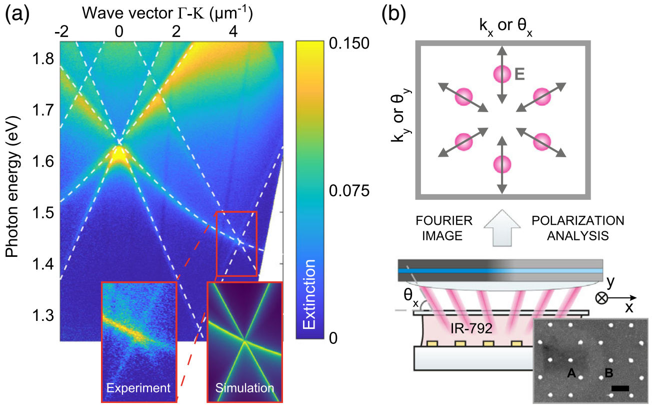

FIG. 1. (a) A measured angle-resolved extinction spectrum of a honeycomb lattice with particle separation of $p = 576$ nm. Color scale shows the extinction which is defined as (1 − normalized transmission). The SLR modes correspond to extinction maxima, closely following the diffracted orders (dashed lines). The left inset shows the measured dispersion around the K point (the color scale is from 0 to 0.05). The right inset shows the dispersion obtained by T-matrix simulations. (b) The lasing measurements. Nanoparticle samples combined with IR-792 molecules in solution are pumped with a femtosecond laser. The hexagonal geometry of the lattice (inset: scanning electron microscope image of the gold nanoparticles, scale bar 500 nm, with the A and B unit cell sites marked) enables lasing emission in six distinct off-normal angles, collected by a 0.6 NA objective and further analyzed. In the Fourier image, the six angles correspond to lasing at the six K points of the first Brillouin zone, with distinct polarization directions (grey arrows) of the electric field $\boldsymbol{E}$.

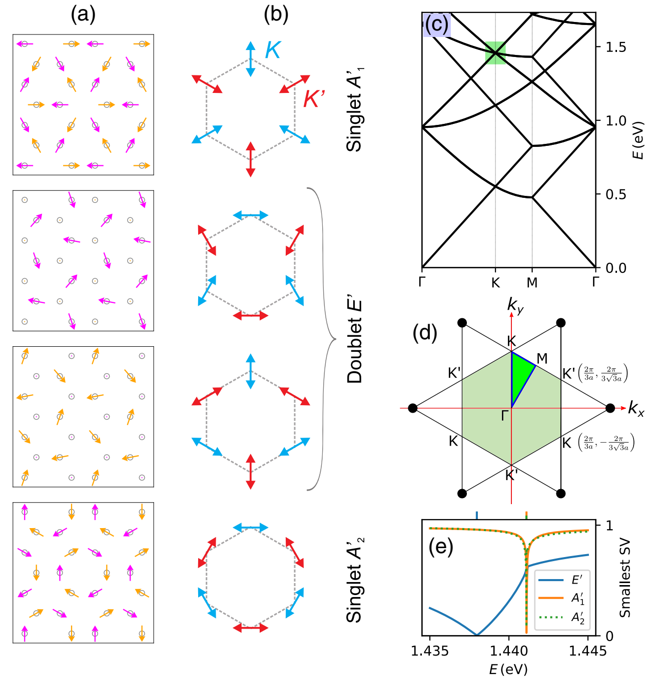

FIG. 2. Eigenmodes of the honeycomb plasmonic lattice at the K point. (a) Real-space electric dipole polarizations of the nanoparticles (circles) corresponding to two singlet modes and a doublet mode, at a specific time. The dipole polarizations depicted by orange and magenta arrows evolve in time rotating clockwise and counterclockwise, respectively, for the K mode, and in the opposite directions for the K' mode. (b) Fourier transform of the dipole polarizations in the corresponding eigenmodes. (c) Band structure of the empty lattice model, that is, as given by diffracted orders of a periodic structure without the effect of the localized plasmonic resonance of the nanoparticles, with the studied K point highlighted. (d) The first Brillouin zone (green area) of the honeycomb reciprocal lattice and its high symmetry points, a is the lattice constant. (e) Singular values (SV) of the symmetry-adapted scattering problem at the K point, whose minima give the mode energies, as function of energy. The color shows the results of projection of the corresponding eigenmodes on the singlets and doublets obtained by group theory (the singlet A_1' that was found to lase experimentally is shown in orange, the other singlet A_2' in green, and the doublet E' in blue), the energies are marked by ticks.

The geometry of an infinite honeycomb lattice belongs to the group $p6m \times \sigma_h$, the wallpaper group $p6m$ [52] extended by the horizontal reflection σ_h. The horizontal reflection ensures that the eigenmodes can be divided into two classes according to the electric field orientation at the mirror plane: the electric field $\boldsymbol{E}$ is either parallel (in plane $\boldsymbol{E}$, the magnetic field $\boldsymbol{H}$ is then perpendicular to the mirror plane) or perpendicular (perpendicular $\boldsymbol{E}$, magnetic field $\boldsymbol{H}$ in plane) [8].

A single unit cell of the reciprocal lattice of our system contains six high symmetry points [Fig. 2(d)]: one Γ point with D_6 point symmetry, as well as two K points with D_3 and three M points with D_2 point symmetries. The K points are mutually related by parity inversion symmetry. Whenever the distinction between the two K points is relevant, we label the other one as K'. To a large extent, group theory determines the properties of the eigenmodes supported at the high-symmetry points. As the reciprocal lattice has D_3 point group symmetry around the K points, the K-point modes must constitute irreducible representations of the D_3 group. Using standard group-theoretical reduction methods [53], we can determine for instance the electric dipole polarizations of the nanoparticles in the respective modes. The irreducible representations of D_3 are either one- or two-dimensional, so the eigenmodes are, apart from accidental degeneracies, either nondegenerate (“singlets,” 1D representation) or doubly degenerate (“doublets,” 2D representation). Six dispersion branches meet at the K point (see Supplemental Material [39]), and the eigenmodes constitute two singlets and two doublets.

Figure 2(a) shows the admissible patterns of nontrivial nanoparticle dipole polarizations in the in plane $\boldsymbol{E}$ case for the singlets and one doublet. Any linear combination of the depicted doublet states is possible as well. Figure 2(b) shows spatial Fourier transforms of these patterns, corresponding to the polarizations of the far-field beams escaping the array.

In real space, the magenta color in Fig. 2 means clockwise rotating electric dipole polarizations while orange means the dipoles rotate counterclockwise for all K modes. For K' modes, the polarization rotation directions are reversed. If the system is excited simultaneously in the K and corresponding K' states with the same intensities, the polarizations will, instead of rotating, oscillate in a linear direction, with the exact direction depending on the relative phase between the K and K' modes. This will be important in analyzing the experimental real-space images.

To characterize the lasing action, we perform angle, energy, polarization, and position resolved emission measurements. Above a critical pump threshold, the sample exhibits an intense and narrow emission peak at 1.426 eV and $k_y \sim 4.25 \times 10^6\ \mathrm{m}^{-1}$ (corresponding to an angle of $35° \pm 0.4°$ with respect to the sample normal), see Figs. 3(a)–3(c). The emission intensity and mode line width as a function of pump fluence is shown in Fig. 3(b). Over three orders of magnitude increase in emission intensity can be seen upon the onset of lasing, typical for nanoparticle arrays with small spontaneous emission coupling to the lasing mode (small β factor [54]) [24,26,28,29,31]. Increased temporal coherence due to lasing is evident from the line width of the emission (2 meV), which is well below the natural line width of the SLR mode at the K point (~20 meV). The 2 meV line width is smaller than those in Refs. [18,21,22,26,31,32] (3.6–27 meV), but larger than the values 0.26–1.5 meV in Refs. [20,24,25,28,29].

In Fig. 4(a), we show the angle resolved emission of the sample. The system exhibits lasing at six specific angles that correspond to three K and three K' points of the lattice. We measure the polarization properties of each point by recording the emission intensities with several different linear polarizer angles. For each point, we recover a typical dipolar emission pattern; however, the direction of linear polarization is different; see Fig. 4(b). The results match excellently the calculated angular distributions of linearly polarized light having a polarization along the six Γ–K directions (the red dashed lines). We find that the A_1' singlet mode has corresponding polarization properties, see Fig. 2(b). The linear polarization degree $\rho_\mathrm{L} = (I_\mathrm{max} - I_\mathrm{min})/(I_\mathrm{max} + I_\mathrm{min})$ reaches on average 0.8 for the six K points.

The identification of the lasing mode as the singlet A_1' can be further confirmed by analyzing the real-space images with variously oriented polarization filters at the output. While the dipole polarization directions of the nanoparticles cannot be measured directly, we can estimate them using the spatial intensity variations due to wave interference in case of different filter orientations. The intensity variations should be most clear in the case where the system lases in the K and K' modes simultaneously, with a fixed (modulo $\pi/3$) relative phase such that the dipoles are oriented as in Fig. 2(a). If the system lases only in one of the K or K' modes, or if the relative phase is random, the real-space intensity distribution should become more uniform due to time averaging (see Supplemental Material [39]).

Figure 5 shows an image of a small piece of the array for three choices of polarization filters for the lasing emission, with the predicted intensities and nanoparticle electric dipole polarizations of the singlet mode A_1' for the ideal, namely zero phase-difference combination of the K and K' modes, as defined in Fig. 2(a) (cases with other polarization filter orientations and details of the theoretical predictions are shown in Supplemental Material [39]). The intensity maxima appear at the places where the surrounding adjacent dipoles, or their projections according to the polarization filter orientation, have the same or similar directions and therefore interfere constructively. Comparing the real-space

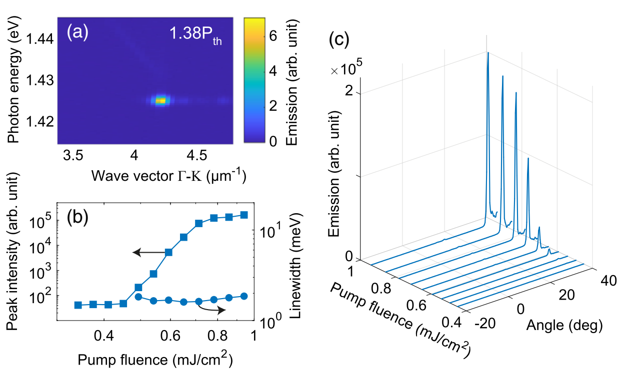

FIG. 3. (a) Measured emission spectra of a honeycomb lattice with $P = 1.38P_\mathrm{th}$, where $P_\mathrm{th} = 0.47\ \mathrm{mJ/cm^2}$ is the threshold pump fluence for the K-point lasing mode (particle distance $p = 576$ nm and diameter $d = 100$ nm). (b) The mode output power (squares) and the line width (circles) at the K-point angle ($35° \pm 0.4°$) as a function of pump fluence. Note that due to low intensity, we cannot determine the line width at pump fluences below the threshold, for below threshold emission, see Supplemental Material [39]. (c) The emission intensity as a function of angle at the K-point energy (~1.426 eV) with several pump fluences.

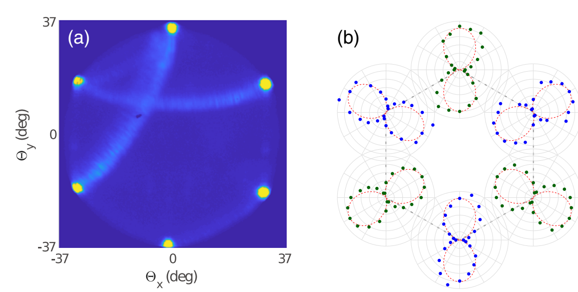

FIG. 4. Lasing mode polarization. (a) Angle resolved emission of the sample without any polarizer in detection. All six K points are clearly visible. (b) Polar emission intensities at each K point in the presence of a linear polarizer. The angles refer to the polarizer angles and the radii refer to the measured intensities. The red dashed lines are the calculated intensity distributions for linearly polarized light (along the Γ–K directions) passing through the polarizer at the corresponding angle.

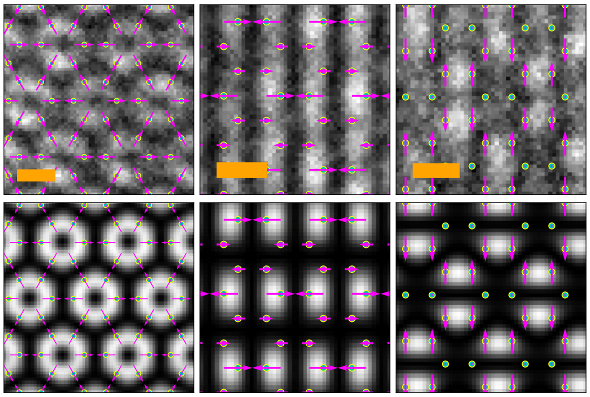

FIG. 5. Upper row: examples of real-space images for different polarization filters (no filter, horizontal, vertical) used for the analysis of the lasing mode. In each case, the expected positions of the nanoparticles (small yellow-cyan circles) and the dipole polarizations (arrows) of the singlet mode A_1' for the ideal (zero) K–K' relative phase are depicted, projected to the corresponding filter direction. Lower row: theoretical prediction for the intensities for the ideal K–K' relative phase. The scale bar length is 1 μm. For images over larger areas, see Supplemental Material [39].

images with dipole orientations predicted for the other modes (A_2' and the doublet E') results in inconsistencies (for details, see Supplemental Material [39]). This confirms that the system indeed lases in the singlet mode A_1'. The intensity variations in the observed patterns show that the system lases in the K and K' singlet A_1' modes simultaneously, with comparable intensities and with a fixed, or at least strongly correlated, relative phase. The existence of interference patterns over the whole sample, furthermore, proves the spatial coherence of the observed lasing. Since the K point of our system corresponds to the crossing of diffractive orders in three directions with 120° angles between them, the feedback in the lasing action is two dimensional, different from one dimensional DFB lasing [2] in nanoparticle arrays [24,25,28,55]. This is reflected in the nontrivial 2D polarization patterns.

DFB-type lasing typically occurs at a band edge or an extremum of the dispersion because zero group velocity enables feedback. Both the measured and simulated dispersions [Fig. 1(a)] show crossings of the modes at the K point, without any visible gap and zero group velocity point. Why does a mode of a certain symmetry (the A_1' singlet) lase, if the K point apparently has a degeneracy of several modes? To answer this we computed the energies of the eigenmodes using symmetry-adapted T-matrix simulations (for details, see Supplemental Material [39]). Figure 2(e) shows that indeed there is a difference in the energies of the A_1' singlet and the E' doublet near the K point. This band gap means that the singlet A_1' has an energy minimum at the K point, which explains why lasing is possible in this mode. The narrower peak for A_1' compared to that for E' indicates higher quality factor, making the former mode more amenable for lasing. The A_2' singlet mode seems almost degenerate with A_1' but the resonance is a bit weaker {slightly smaller dip in Fig. 2(e); see Supplemental Material [39] for a larger picture}. The energy difference between A_1' and E' is only 3.2 meV, smaller than the natural linewidth of the SLR mode around 20 meV, which explains why the gap is not visible in the dispersions. On the other hand, the lasing emission has 2 meV linewidth, similar to the scale of the band gap.

In summary, we have observed lasing action at the K and K' points of a honeycomb plasmonic lattice. Both the polarization of the six output beams and the real space interference patterns provide distinct features that, when combined with the group theory description, reveal the lasing mode as the singlet A_1'. Analysis of the T-matrix simulation results using the group theory eigenmodes showed that the singlet A_1' has an energy minimum at the K point, which enables the feedback necessary for lasing. Our results demonstrate the potential of plasmonic nanoparticle array systems for tailoring the polarization and beam direction of laser output by the lattice geometry. The tunability of the beam direction (here ~35°) can be used for bringing the beam close to the in plane direction. If realized in a less lossy platform, this could enable on-chip planar integration.

Our study gives a promising starting point for investigations of topological photonics and lasing [7,56–63] in radiatively coupled systems. Plasmonic nanoparticle array lasers offer a unique combination of easy fabrication, room temperature operation, ultrafast speeds, long-range radiative coupling, and strong coupling to emitters (the gain medium) [26,64,65]. Radiatively coupled systems offer topological phenomena different from tight-binding models [66]. Arrays of magnetic nanoparticles have been realized [67], and the magnetization of nanoparticles could be used for opening topological gaps at the high-symmetry points where we have shown lasing. Time reversal symmetry breaking is one of the main mechanisms leading to topologically nontrivial systems but topological gaps based on magnetic materials [62,63] are extremely small at optical frequencies [56]. The polarization and interference analysis demonstrated here should prove helpful in identifying topological modes, and the observed stability of the lasing action despite a narrow gap is promising concerning topological lasing relying on small topological gaps.

This work was supported by the Academy of Finland through its Centres of Excellence Programme (Projects No. 284621, No. 303351, No. 307419) and by the European Research Council (Grant No. ERC-2013-AdG-340748-CODE). This work benefited from discussions and visits within the COST Action MP1403 Nanoscale Quantum Optics, supported by COST (European Cooperation in Science and Technology). Part of the research was performed at the Micronova Nanofabrication Centre, supported by Aalto University. Computing resources were provided by the Triton cluster at Aalto University. The authors thank Matthias Saba, Ortwin Hess, Tero Heikkilä, and Heikki Rekola for fruitful discussions.

*paivi.torma@aalto.fi

[1] F. Koyama, S. Kinoshita, and K. Iga, Appl. Phys. Lett. **55**, 221 (1989).
[2] H. Kogelnik and C. V. Shank, J. Appl. Phys. **43**, 2327 (1972).
[3] J. P. Dowling, M. Scalora, M. J. Bloemer, and C. M. Bowden, J. Appl. Phys. **75**, 1896 (1994).
[4] M. Meier, A. Mekis, A. Dodabalapur, A. Timko, R. E. Slusher, J. D. Joannopoulos, and O. Nalamasu, Appl. Phys. Lett. **74**, 7 (1999).
[5] S. Noda, M. Yokoyama, M. Imada, A. Chutinan, and M. Mochizuki, Science **293**, 1123 (2001).
[6] H. Matsubara, S. Yoshimoto, H. Saito, Y. Jianglin, Y. Tanaka, and S. Noda, Science **319**, 445 (2008).
[7] T. Ozawa, H. M. Price, A. Amo, N. Goldman, M. Hafezi, L. Lu, M. Rechtsman, D. Schuster, J. Simon, O. Zilberberg, and I. Carusotto, arXiv:1802.04173.
[8] M. S. Dresselhaus, G. Dresselhaus, and A. Jorio, *Group Theory: Application to the Physics of Condensed Matter* (Springer, Berlin, Heidelberg, 2008).
[9] G. Weick, C. Woollacott, W. L. Barnes, O. Hess, and E. Mariani, Phys. Rev. Lett. **110**, 106801 (2013).
[10] M. C. Rechtsman, J. M. Zeuner, Y. Plotnik, Y. Lumer, D. Podolsky, F. Dreisow, S. Nolte, M. Segev, and A. Szameit, Nature (London) **496**, 196 (2013).
[11] T. Jacqmin, I. Carusotto, I. Sagnes, M. Abbarchi, D. D. Solnyshkov, G. Malpuech, E. Galopin, A. Lemaître, J. Bloch, and A. Amo, Phys. Rev. Lett. **112**, 116402 (2014).
[12] S. Bittner, B. Dietz, M. Miski-Oglu, P. Oria Iriarte, A. Richter, and F. Schäfer, Phys. Rev. B **82**, 014301 (2010).
[13] M. Bellec, U. Kuhl, G. Montambaux, and F. Mortessagne, Phys. Rev. Lett. **110**, 033902 (2013).
[14] C. Becker, P. Soltan-Panahi, J. Kronjäger, S. Dörscher, K. Bongs, and K. Sengstock, New J. Phys. **12**, 065025 (2010).
[15] Z. Chen and B. Wu, Phys. Rev. Lett. **107**, 065301 (2011).
[16] J. Struck, M. Weinberg, C. Ölschläger, P. Windpassinger, J. Simonet, K. Sengstock, R. Höppner, P. Hauke, A. Eckardt, M. Lewenstein, and L. Mathey, Nat. Phys. **9**, 738 (2013).
[17] T. Li, L. Duca, M. Reitter, F. Grusdt, E. Demler, M. Endres, M. Schleier-Smith, I. Bloch, and U. Schneider, Science **352**, 1094 (2016).
[18] W. Zhou, M. Dridi, J. Y. Suh, C. H. Kim, D. T. Co, M. R. Wasielewski, G. C. Schatz, and T. W. Odom, Nat. Nanotechnol. **8**, 506 (2013).
[19] F. van Beijnum, P. J. van Veldhoven, E. J. Geluk, M. J. A. de Dood, G. W. 't Hooft, and M. P. van Exter, Phys. Rev. Lett. **110**, 206802 (2013).
[20] X. Meng, J. Liu, A. V. Kildishev, and V. M. Shalaev, Laser Photonics Rev. **8**, 896 (2014).
[21] A. H. Schokker and A. F. Koenderink, Phys. Rev. B **90**, 155452 (2014).
[22] A. Yang, T. B. Hoang, M. Dridi, C. Deeb, M. H. Mikkelsen, G. C. Schatz, and T. W. Odom, Nat. Commun. **6**, 6939 (2015).
[23] J. Cuerda, F. Rüting, F. J. García-Vidal, and J. Bravo-Abad, Phys. Rev. B **91**, 041118 (2015).
[24] T. K. Hakala, H. T. Rekola, A. I. Väkeväinen, J.-P. Martikainen, M. Nečada, A. J. Moilanen, and P. Törmä, Nat. Commun. **8**, 13687 (2017).
[25] D. Wang, A. Yang, W. Wang, Y. Hua, R. D. Schaller, G. C. Schatz, and T. W. Odom, Nat. Nanotechnol. **12**, 889 (2017).
[26] M. Ramezani, A. Halpin, A. I. Fernández-Domínguez, J. Feist, S. R. -K. Rodriguez, F. J. Garcia-Vidal, and J. G. Rivas, Optica **4**, 31 (2017).
[27] A. H. Schokker, F. van Riggelen, Y. Hadad, A. Alù, and A. F. Koenderink, Phys. Rev. B **95**, 085409 (2017).
[28] H. T. Rekola, T. K. Hakala, and P. Törmä, ACS Photonics **5**, 1822 (2018).
[29] K. S. Daskalakis, A. I. Väkeväinen, J.-P. Martikainen, T. K. Hakala, and P. Törmä, Nano Lett. **18**, 2658 (2018).
[30] V. T. Tenner, M. J. A. d. Dood, and M. P. v. Exter, Opt. Lett. **43**, 166 (2018).
[31] H.-Y. Wu, L. Liu, M. Lu, and B. T. Cunningham, Adv. Opt. Mater. **4**, 708 (2016).
[32] C. Zhang, Y. Lu, Y. Ni, M. Li, L. Mao, C. Liu, D. Zhang, H. Ming, and P. Wang, Nano Lett. **15**, 1382 (2015).
[33] J.-P. Martikainen, M. O. J. Heikkinen, and P. Törmä, Phys. Rev. A **90**, 053604 (2014).
[34] T. K. Hakala, A. J. Moilanen, A. I. Väkeväinen, R. Guo, J.-P. Martikainen, K. S. Daskalakis, H. T. Rekola, A. Julku, and P. Törmä, Nat. Phys. **14**, 739 (2018).
[35] M. Notomi, H. Suzuki, and T. Tamamura, Appl. Phys. Lett. **78**, 1325 (2001).
[36] S. W. Chen, T. C. Lu, Y. J. Hou, T. C. Liu, H. C. Kuo, and S. C. Wang, Appl. Phys. Lett. **96**, 071108 (2010).
[37] W. Huang, D. Pu, W. Qiao, W. Wan, Y. Liu, Y. Ye, S. Wu, and L. Chen, J. Phys. D **49**, 335103 (2016).
[38] N. Y. Kim, K. Kusudo, A. Löffler, S. Höfling, A. Forchel, and Y. Yamamoto, New J. Phys. **15**, 035032 (2013).
[39] For Supplemental Material, see http://link.aps.org/supplemental/10.1103/PhysRevLett.122.013901 for technical details about the experimental setup and the theoretical methods used.
[40] J. Thompson, M. Anni, S. Lattante, D. Pisignano, R. Blyth, G. Gigli, and R. Cingolani, Synth. Met. **143**, 305 (2004).
[41] D. W. Mackowski, Proc. R. Soc. A **433**, 599 (1991).
[42] F. M. Schulz, K. Stamnes, and J. J. Stamnes, J. Opt. Soc. Am. A **16**, 853 (1999).
[43] H. Reid, SCUFF-EM, http://github.com/homerreid/scuff-EM.
[44] M. T. H. Reid and S. G. Johnson, IEEE Trans. Antennas Propag. **63**, 3588 (2015).
[45] P. B. Johnson and R. W. Christy, Phys. Rev. B **6**, 4370 (1972).
[46] G. Kristensson, *Scattering of Electromagnetic Waves by Obstacles* (SciTech Publishing, Edison, NJ, 2016).
[47] Y.-l. Xu, J. Comput. Phys. **139**, 137 (1998).
[48] C. Linton, SIAM Rev. **52**, 630 (2010).
[49] S. Zou and G. C. Schatz, Chem. Phys. Lett. **403**, 62 (2005).
[50] W. Wang, M. Ramezani, A. I. Väkeväinen, P. Törmä, J. G. Rivas, and T. W. Odom, Mater. Today **21**, 303 (2018).
[51] R. Guo, T. K. Hakala, and P. Törmä, Phys. Rev. B **95**, 155423 (2017).

[52] T. Hahn, *International Tables for Crystallography, Vol. A: Space Group Symmetry*, 5th ed., IUCr Series. International Tables of Crystallography (Springer, Dordrecht, 2002).
[53] J. D. Dixon, Math. Comput. **24**, 707 (1970).
[54] G. Björk and Y. Yamamoto, IEEE J. Quantum Electron. **27**, 2386 (1991).
[55] D. Wang, W. Wang, M. P. Knudson, G. C. Schatz, and T. W. Odom, Chem. Rev. **118**, 2865 (2018).
[56] B. Bahari, A. Ndao, F. Vallini, A. E. Amili, Y. Fainman, and B. Kanté, Science **358**, 636 (2017).
[57] A. B. Khanikaev and G. Shvets, Nat. Photonics **11**, 763 (2017).
[58] G. Harari, M. A. Bandres, Y. Lumer, M. C. Rechtsman, Y. D. Chong, M. Khajavikhan, D. N. Christodoulides, and M. Segev, Science **359**, eaar4003 (2018).
[59] M. A. Bandres, S. Wittek, G. Harari, M. Parto, J. Ren, M. Segev, D. N. Christodoulides, and M. Khajavikhan, Science **359**, eaar4005 (2018).
[60] L. Lu, J. D. Joannopoulos, and M. Soljačić, Nat. Photonics **8**, 821 (2014).
[61] L. Lu, J. D. Joannopoulos, and M. Soljačić, Nat. Phys. **12**, 626 (2016).
[62] F. D. M. Haldane and S. Raghu, Phys. Rev. Lett. **100**, 013904 (2008).
[63] S. Raghu and F. D. M. Haldane, Phys. Rev. A **78**, 033834 (2008).
[64] A. I. Väkeväinen, R. J. Moerland, H. T. Rekola, A.-P. Eskelinen, J.-P. Martikainen, D.-H. Kim, and P. Törmä, Nano Lett. **14**, 1721 (2014).
[65] P. Törmä and W. L. Barnes, Rep. Prog. Phys. **78**, 013901 (2015).
[66] S. R. Pocock, X. Xiao, P. A. Huidobro, and V. Giannini, ACS Photonics **5**, 2271 (2018).
[67] M. Kataja, T. K. Hakala, A. Julku, M. J. Huttunen, S. van Dijken, and P. Törmä, Nat. Commun. **6**, 7072 (2015).